Grid-Feeding Inverter with Simplified Virtual Synchronous Compensator Providing Grid Services and Grid Support

Grid-Feeding Inverter with Simplified Virtual Synchronous Compensator Providing Grid Services and Grid Support

Fabio Mandrile, *Student Member IEEE*, Enrico Carpaneto, *Member IEEE* and Radu Bojoi, *Fellow IEEE*
Dipartimento Energia "G. Ferraris", Politecnico di Torino, Torino, Italy

***Abstract*—This paper proposes the enhancement of the control of a grid-connected inverter by a Simplified Virtual Synchronous Compensator (S-VSC) model working in parallel with the traditional inverter current control loops. The goal of the integration of this model into the inverter control scheme is to provide grid services, such as virtual inertia behavior, current harmonic compensation, as well as reactive grid support during faults. The S-VSC is only in charge of providing the aforementioned services, working therefore always at a low power level. On the other hand, the main power references are sent directly to the inverter control loops. This way, a more stable and damped operation of the inverter is obtained. The proposed structure has been implemented on a 15 kVA grid-connected inverter for experimental validation.**

***Index Terms*—Virtual Synchronous Machines (VSMs), Renewable Energy Sources, (RESs), Virtual Inertia, Grid-Connected Inverter, Grid Services, Grid Support.**

I. Introduction

IN the next 20 years, the amount of energy generation from Renewable Energy Sources (RESs) is expected to rise exponentially all over the world [1]. The most promising RESs are sun and wind. Such resources are interfaced to the electric grid by means of power electronic converters. Traditionally, such converters are operated according to a Maximum Power Point (MPP) strategy, trying to exploit the RES at its maximum. This kind of control may not be feasible in the future, if the penetration of inverter-based generation in the electric grid reaches higher levels. In fact, inverters will be required to provide ancillary services that are traditionally in charge of synchronous generators. The ancillary services include transient support to the grid during sudden frequency changes (inertial behavior [2]), reactive support during voltage dips, harmonic compensation and islanding capabilities [3].

To provide the aforementioned services, a promising idea is to control grid-tied inverters to make them behave as synchronous machines. Several different models have been proposed to provide some or all such services. Among them, the literature reports the Virtual Synchronous Machine (VISMA) [4]–[6], the Synchronverter [7], [8], the Cascaded Virtual Synchronous Machine (CVSM) [9], Kawasaki Heavy Industries (KHI) model [17], Virtual Synchronous Generators (VSGs) [10], [11] and the Synchronous Power Controller (SPC) [12]–[14].

This paper proposes an S-VSC model to provide grid services and grid support. Its peculiar parallel integration with a traditional inverter control structure is described and discussed.

The proposed S-VSC model inherits the following beneficial features already existing in the literature:

- Traditional **current control** to have a straightforward **current limitation** during faults. Any current control strategy available in the literature can be employed, as in the CVSM and the SPC;
- The S-VSC is used as source of grid synchronization. So no PLL is needed, as in SPC, Synchronverter, VISMA and some VSGs. This feature guarantees **less sensitivity** to harmonic distortion in the grid and **reduces the risk** of loss of synchronization during grid faults.

Moreover, with respect to previous models, the proposed solutions has the following benefits:

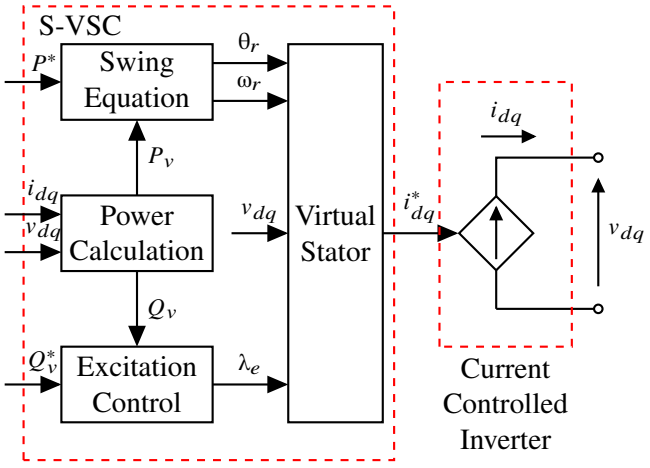

Fig. 1. Block diagram of the proposed S-VSC controlling a grid-feeding inverter.

- The damping of the S-VSC is done using only an equivalent q-axis damper winding as in [15]. Therefore, the **damping** is fully **independent and decoupled from the primary regulation of the frequency**. Full dampers model have already been used in the VISMA [4]. In the proposed model, a **simplified damper** is adopted, in order to ensure the same performance, but at a reduced complexity.
- The S-VSC generates **additive power contributions** to the inverter references, to guarantee **grid services** (inertia emulation and compensation of current harmonics) and **grid support** during symmetrical and asymmetrical faults with reactive power only. In the literature, however, the virtual machines are always in charge of processing the full power references. Therefore the S-VSC always operates at low load, featuring **higher transient stability** and damping;
- The compensating references of the S-VSC can be therefore enabled/disabled or a single channel (active or reactive) can be used, depending on the users' needs. This solution is therefore more flexible and modular in comparison with existing literature.

This paper is an extension of [16], where the S-VSC model was preliminary presented and analyzed. In particular, the following additions have been made:

- A section focusing on tunable harmonic compensation has been added;
- A comparison of the harmonic compensation capabilities with the KHI model [17] has been included;
- A description of the experimental implementation of the startup and synchronization process has been added;
- Additional experimental results have been included and the reference list has been enhanced.

This paper is organized as follows. In Section II the proposed model is presented. Section III describes how the proposed S-VSC model is integrated into the inverter control structure. The experimental validation of the proposed solution is available in Section IV.

II. S-VSC Model

A. Electromechanical Model

The S-VSC is a Virtual Synchronous Machine (VSM) that represents an equivalent linear and isotropic Synchronous Generator (SG) with round rotor, a single damper winding and having one pole pair. The iron losses are neglected. The S-VSC is expressed in the rotor (d, q) synchronous frame. The q-axis leads the d-axis by 90°.

The proposed model is a voltage-input, power-output model, as shown in Fig.1. The input voltage v_{dq} is the sampled grid voltage at the Point of Common Coupling (PCC). The output of the model are the S-VSC active and reactive power P_v, Q_v.

The virtual rotor and the machine virtual windings are depicted in Fig. 2. The machine subtransient inductances $L_d^{"}$ and $L_q^{"}$ are equal (i.e. subtransient isotropic machine) to L_s. The damper winding is acting only in the q-axis and denoted with the suffix rq as in [15]. The excitation of the machine is represented by an ideal excitation winding, providing the desired flux linkage λ_e without any delay related to the excitation circuit.

Every equation is expressed in per unit. V_b is the base voltage (peak value of the phase voltage), S_b is the base power and ω_b is the base speed.

The equivalent electrical circuits of the S-VSC are depicted in Fig. 3 (d-axis) and Fig. 4 (q-axis) [15]. Such equivalent circuits are a simplified version of the traditional modeling of synchronous alternators [18]. The non ideal and not strictly necessary features for the desired goals stated in the Introduction (such as dampers in both axes) have been excluded. The resulting electrical equations of the virtual machine are as follows:

$$\begin{aligned} v_d &= -R_s i_d - \omega_r \lambda_q + \frac{1}{\omega_b}\frac{d\lambda_d}{dt} \\ v_q &= -R_s i_q + \omega_r \lambda_d + \frac{1}{\omega_b}\frac{d\lambda_q}{dt} \\ \tau_{rq0}\frac{d\lambda_{rq}}{dt} &= -\lambda_{rq} - L_{rq} i_q \\ \tau_{rq0} &= \frac{L_{rq}}{\omega_b R_{rq}} \end{aligned} \tag{1}$$

where R_s is the stator virtual resistance, λ_d and λ_q are the virtual stator flux linkages, λ_{rq} the damper winding flux linkage and ω_r the virtual rotor speed; R_{rq}, L_{rq} and τ_{rq0} are the parameters of the q-axis virtual damper winding [15].

The virtual currents i_{dq} of the S-VSC can be calculated through the inverse magnetic model of the machine as follows:

$$\begin{aligned} i_d &= \frac{\lambda_e - \lambda_d}{L_d^{"}} \\ i_q &= \frac{\lambda_{rq} - \lambda_q}{L_q^{"}} \end{aligned} \tag{2}$$

The mechanical part of the S-VSC is a simplified swing equation and does not include a mechanical damping term as in other solutions available in the literature [7], [9], but is provided in the electrical part by the q-axis simplified virtual damper. The block diagram of

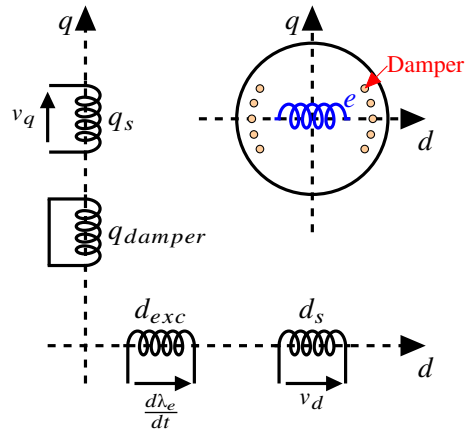

Fig. 2. Winding diagram and rotor section of the S-VSC in the rotor (d,q) frame. d_s and q_s are the stator windings, q_{damper} and d_{exc} the rotor windings. They represent the q-axis damper and an equivalent winding of the excitation, respectively.

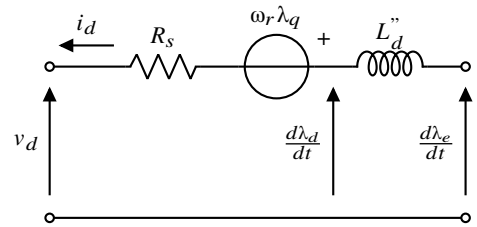

Fig. 3. d-axis equivalent circuit.

the mechanical part is shown in Fig. 5. The resulting mechanical equations are expressed as:

$$\begin{aligned} P_v^* - P_v &= 2H\frac{d\omega_r}{dt} \\ \frac{d\theta_r}{dt} &= \omega_r \cdot \omega_b \end{aligned} \tag{3}$$

where P_v^* is the virtual mechanical power reference provided to the virtual machine, P_v the actual active power of the S-VSC, H is the inertia constant of the virtual machine and θ_r is the position of the virtual rotor (i.e. the position of the (d,q) reference frame).

Finally, the excitation control of the S-VSC acts as a simple integral controller on the reactive current of the machine as follows:

$$\lambda_e = \int k_e \frac{Q_v^* - Q_v}{V_g} dt \tag{4}$$

where k_e is the excitation gain, Q_v^* is the reactive power reference given to the VSG, Q_v is the actual reactive power of the VSG and V_g the peak value of the input grid voltage.

The excitation gain can be tuned in first approximation according to:

$$k_e = \frac{L_s + L_g^{est}}{\tau_e} \tag{5}$$

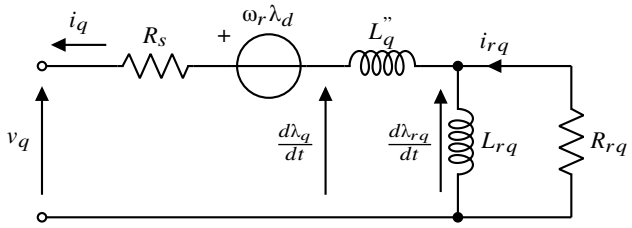

Fig. 4. q-axis equivalent circuit [15].

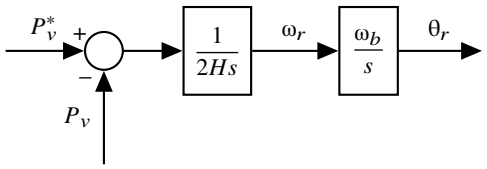

Fig. 5. Simplified swing equation of the S-VSC.

where L_g^{est} is the estimated grid inductance and τ_e is the desired time constant of the reactive control.

The per unit active and reactive power of the S-VSC are calculated according to the instantaneous power theory as:

$$P_v + j \cdot Q_v = \left(v_d + j \cdot v_q\right)\left(i_d - j \cdot i_q\right) \tag{6}$$

As mentioned in the introduction, the S-VSC always operates with zero power references (i.e. $P_v^* = Q_v^* = 0$). From the load angle characteristic [18] depicted in Fig. 6, the stable operating region of a synchronous machine corresponds to a load angle interval comprised between $\pi/2$ and $-\pi/2$. While VSGs usually operate over all this stable region, changing radically their load angle according to the needed active power, the S-VSC always operates around the point $\delta = 0$. Therefore, when the active power transfer to the grid changes, only the converter control loops change their operating point. On the other hand, the S-VSC does not change its load angle, since it operates in parallel with the converter, similarly to a synchronous condenser. Therefore, also the virtual speed ω_r does not change significantly. Therefore leading to a better quality of the grid frequency using the S-VSC even during load transients. Moreover, this leads to improved both small signal and large signal stability [18], as more angle margin during grid faults is available.

B. Operating Modes

Even though the S-VSC operates always with zero active and reactive power references, three operating modes listed in Table I can be defined.

The difference between the three operating modes consists in where the power references P^* and Q^* are fed. Such references can be either provided directly to the inverter control loops or given as references to the

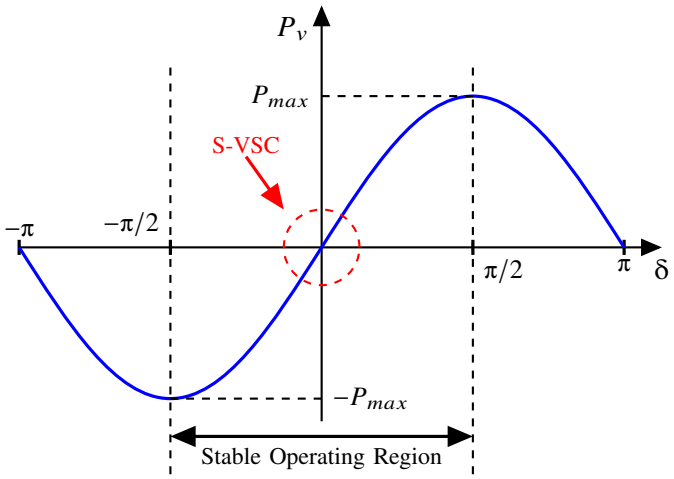

Fig. 6. Power angle relationship of a SG to highlight the operating area of S-VSC.

TABLE I. Operating modes of the S-VSC.

Mode	P*	Q*
VSC (Virtual Synchronous Compensator)	Inverter	Inverter
VSCap (Virtual Synchronous Condenser)	Inverter	VSM
VSG (Virtual Synchronous Generator)	VSM	VSM

VSM. This paper does not deal with the calculation of such references and they are assumed to be calculated by an higher level control logic.

The proposed and fully described operating mode is the VSC. In this operating mode, the power references are processed directly by the inverter control loops and the virtual machine is only in charge of generating compensation references to provide grid ancillary services (virtual inertia, reactive support, harmonic compensation).

The second operating mode is the Virtual Synchronous Condenser (VSCap). Here, the VSM is in charge of processing the reactive power references Q^*. This mode is the most similar to the physical synchronous condensers employed in the power grid.

The last operating mode is the VSG, meaning that the VSM fully operates as a real synchronous generator, processing both active and reactive power references. In this case, the inverter control loops simply track the references generated by the VSG. The definition of such operating modes is useful to compare the proposed solution with other models existing in the technical literature, which can be classified as VSGs. In the experimental section these three modes will be compared.

C. Tunable Harmonic Compensation

The virtual stator embeds also a harmonic compensation feature. As in real synchronous machines, the S-VSC is able to generate current reference to counteract

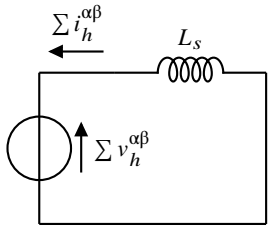

Fig. 7. Equivalent circuit at steady state for harmonic compensation in the equivalent (α,β) frame.

harmonic distortions in the power grid. The virtual stator can be modeled in the stationary (α,β) frame as in Fig. 7. In fact, at steady state it acts as a virtual inductance L_s (the resistance R_s is usually much lower and is therefore neglected). This virtual stator circuit at steady state, when supplied by a grid voltage including n arbitrary harmonic distortions of order h, generates harmonic current references that are as follows in the stationary (α,β) frame:

$$i_h^{\alpha\beta} = \frac{v_h^{\alpha\beta}}{h\omega_g L_s}, \quad h = 1 \dots n \tag{7}$$

This means that the S-VSC is able to generate a compensating current, that is inversely proportional to the virtual stator inductance L_s. Since the virtual stator inductance is tunable, the magnitude of the injected current can be varied. It must be noted that a suitable current controller is needed to compensate high order harmonics. This aspect will be further discussed in Section III.

The tunable harmonic compensation feature has been tested in simulation with an existing VSG model: KHI [17]. The following system has been considered:

- A three-phase converter with ideal DC source equipped with an LCL grid-side filter (same parameters as the experimental setup listed in Tab. II);
- A transformer to interface the generating plant with the grid. It has been modeled with its equivalent inductance $L_t = 0.1$ pu;
- Both models have been tuned with equivalent parameters (inertia, damping, virtual stator...);
- The converter was modeled with average values. An accurate modeling of the PWM modulation is in fact not necessary when dealing with lower frequency phenomena, such as the harmonic distortion;
- Both controllers were implemented in digital form and the equivalent delay of the digital controller and PWM modulation was included as well;
- Both systems were equipped with the same current controller, as further explained in Section III and Section IV;

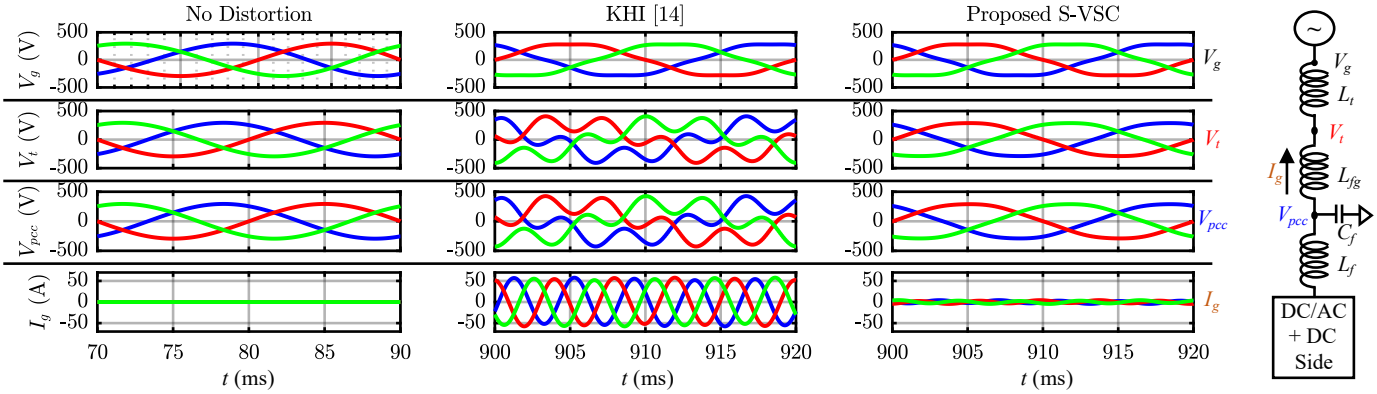

Fig. 8. Simulation comparison of the proposed S-VSC with the existing KHI model. Voltages are line-line.

- Both models were operating at no load in order to clearly identify the differences among them.

To compare the two systems, a 5% 5th harmonic voltage perturbation has been applied to the grid (V_g). The voltage shapes at different points (V_t, V_{pcc}) and the current injected into the grid were compared and the results are displayed in Fig. 8. Both models behave equally under ideal grid conditions (left column), by injecting no current. The voltage is not distorted in any point. When the voltage perturbation is applied (central and right column) both systems inject current at the disturbance frequency. However, the KHI model, being implemented with an algebraic virtual stator, injects very large currents that further contribute to the voltage distortion. On the other hand, the proposed S-VSC (right column) is injecting smaller currents according to (7). Such currents are effective in compensating the voltage distortion. As it can be seen in Fig. 8, both the line-line voltages V_t and V_{pcc} do not feature the typical peak shaving caused by the 5th harmonic, but have a more sinusoidal shape. In Section IV more experimental results are reported for the S-VSC.

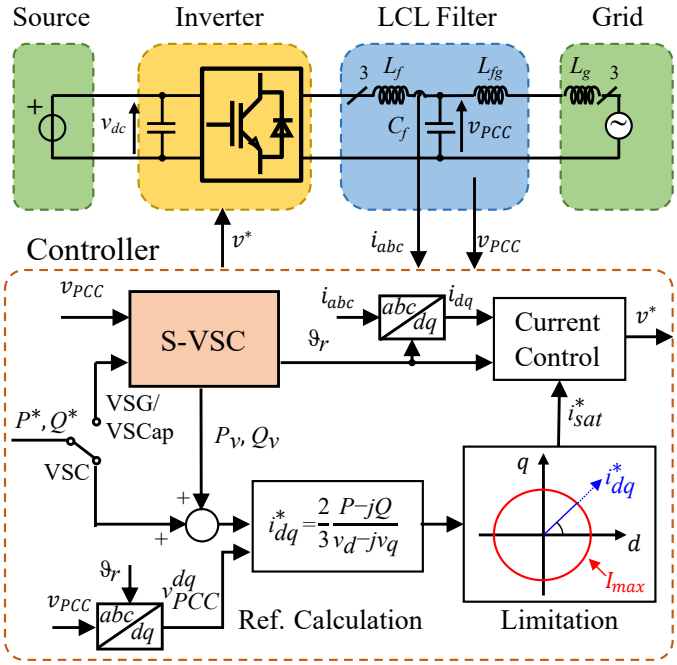

Fig. 9. Diagram of the grid-feeding inverter equipped with the proposed S-VSC.

III. S-VSC Integration in Inverter Control

An inverter connected to the grid by means of an LCL filter, is considered as shown in Fig. 9. The inverter DC link is supplied by a DC source with voltage regulation, that keeps constant the DC voltage.

The inverter control structure is depicted in Fig. 9. The measured quantities are the inverter output current i_{abc}, the line-line voltage across at the filter capacitors v_{PCC} and the DC link voltage v_{dc}.

The external power references (e.g. coming from a grid voltage or frequency control) are directly fed to the inverter control loops, while the virtual machine adds extra power reference terms to compensate any grid perturbation. The inverter control loops are implemented in a rotating (d,q) frame. This frame is aligned to the S-VSC's rotor angle θ_r. In fact, thanks to the inertial effect of the virtual rotor, VSMs embed stable and filtered grid synchronization capabilities. Therefore, they can provide a better angle reference under non-ideal grid conditions (faults, harmonic distortion, phase displacement) compared to a commonly used Phase Locked Loop (PLL).

The S-VSC is initialized by setting the rotor speed $\omega_r = 1$ pu and the virtual flux linkages $\lambda_d = \lambda_e = V_g/\omega_r$, $\lambda_{rq} = \lambda_q = 0$, where V_g is the peak voltage of the grid in pu. The initial rotor angle $\theta_r = 0$. After a short virtual transient, the S-VSC automatically synchronizes to the grid and the current control and the inverter modulation can be enabled safely.

The controlled current is the inverter output current

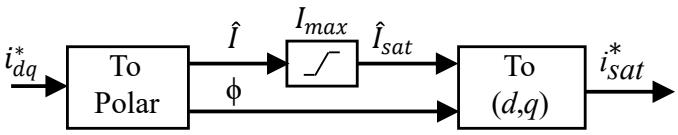

Fig. 10. Current limitation strategy.

i_{abc}, referred to the (*d*,*q*) frame as i_d, i_q. The voltage v_{PCC} is referred to the (*d*,*q*) frame as v_d, v_q.

The current reference vector i^*_{dq} is calculated from the power references P, Q and the measured grid voltage v_d, v_q, as:

$$i^*_{dq} = i^*_d + j i^*_q = \frac{2}{3}\frac{P - jQ}{v_d - jv_q} \tag{8}$$

The amplitude of the reference current vector is limited to comply with the inverter rating even during faults, without modifying its position in the (*d*,*q*) plane. Therefore, the ratio between the active and reactive component of the current are not altered. This saturation strategy is explained in Fig. 10. The current reference vector i^*_{dq} is saturated to the maximum current value I_{max} without altering its phase ϕ. This results in the saturated current reference vector i^*_{sat}.

The current control (Current Control block in Fig. 9) can be performed using any of the existing strategies presented in literature [19], [20]. In this paper, a PI+RES (tuned to the 6th harmonic) controller in the (*d*,*q*) rotating frame as in [21] has been implemented. The tuning of the controller (i.e. the proportional and integral gains k_p and k_i) given the control bandwidth f_{BWi} and the angular frequency of the zero of the PI ω_{zi}, is performed according to the previous literature, to obtain the optimal performance in both steady state and transient operation. If harmonic compensation is needed, then the current controller must be designed in order to track current references different from the fundamental. For example, resonant controllers tuned on the multiples of the fundamental frequency represent a valid solution [19].

IV. Experimental Validation

The proposed S-VSC model and its integration into a grid-feeding converter has been implemented on a 15 kVA grid-connected inverter. Fig. 11 shows a view of the experimental setup. The DC source output is 400 V. The 50 kVA grid emulator provides a 220 Vrms line-line grid voltage at 50 Hz. The entire control algorithm is implemented in C code on a dSPACE 1005 platform. The inverter switching frequency and the sampling frequency are both 10 kHz. The LCL filter parameters as well as the S-VSC parameters are listed in Table II.

The performed tests are the following:

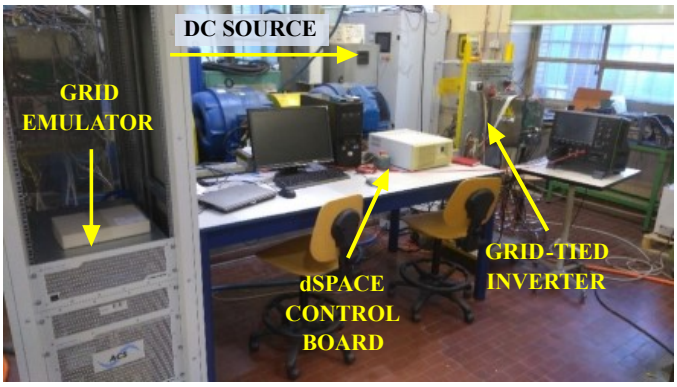

Fig. 11. Experimental setup used for validation.

TABLE II. Inverter and S-VSC parameters for the experimental tests (unless explicitly mentioned otherwise).

Parameter	Value	Parameter	Value
V_b	$120\sqrt{2}$ V	S_b	15 kVA
L_f	545 µH	C_f	22 µF
L_{fg}	120 µH	L_g	270 µH
f_{BWi}	500 Hz	ω_{zi}	314.15 rad/s
k_p	1.712 V/A	k_i	537.9 V/(As)
L_s	0.1 pu	R_s	0.02 pu
H	4 s	τ_e	0.1 s
L_{rq}	0.71 pu	τ_{rq0}	0.23 s

A) Startup and synchronization (Test 1)
B) Inertial behavior tests (Tests 2 and 3)
C) Operating modes comparison (Test 4, 5 and 6)
D) Voltage dip (Tests 7, 8, 9 and 10)
E) Harmonic compensation (Tests 11 and 12)

A. Synchronization and Startup

The synchronization process of VSMs is a crucial aspect, just as the synchronization of real SGs. The advantage of virtual machines is the possibility of having a virtual transient, with no current exchange with the grid. The startup process follows the steps:

1) Start synchronization: the S-VSC is enabled and the model is executed by the digital controller. The current control is in reset state. The PWM modulation is off and the power switches are open. No current is therefore injected;
2) Synchronization: The S-VSC synchronizes to the grid voltage without the need of a PLL. The duration of the transient depends on the initial load angle between the S-VSC and the grid. As it can be seen in Test 1, Fig. 12, any initial load angle does lead to the synchronization. The synchronization ends when the virtual speed ω_r settles to the grid frequency;
3) Start Control: the S-VSC is synchronized and perfectly tracks the grid frequency and phase. The

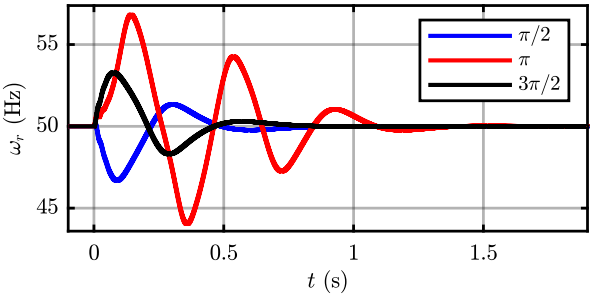

Fig. 12. Test 1: S-VSC synchronization transient with different initial load angles ($\pi/2, \pi, 3\pi/2$).

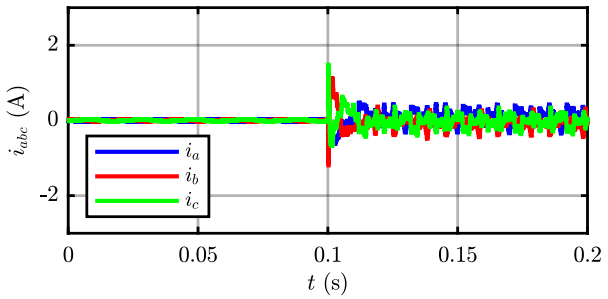

Fig. 13. Test 1: Startup transient. PWM and current control are enabled at t = 0.1 s after the synchronization is completed.

PWM modulation and the current control can be enabled. As Fig. 13 shows, the PWM is enabled at t = 0.1 s after the synchronization is completed. The currents are controlled to be 0 A after startup. The converter is now fully operating, tracking the power references.

The startup process is therefore performed in the time span of few seconds, depending on the initial load angle of the S-VSC. The large virtual speed variations of the S-VSC (more than 5 Hz) during the synchronization process are not an issue, since this phase is performed within the digital control, with no current exchange with the grid. Since the S-VSC operates at no load during the synchronization process, there is no stability boundary on the initial load angle.

B. Inertial Behavior

Tests 2 and 3 highlight the effective inertial behavior of the S-VSC, injecting active power into the grid with the goal of reducing the Rate of Change of Frequency (RoCoF) and increasing the frequency nadir. The results are available in Fig. 14 and Fig. 15. In the first test, a realistic grid frequency profile (e.g. after a major generator disconnection from the grid) is generated by the grid emulator. Its parameters are severe (large frequency derivative, low frequency nadir and low frequency after fault) better to highlight the active power injected from

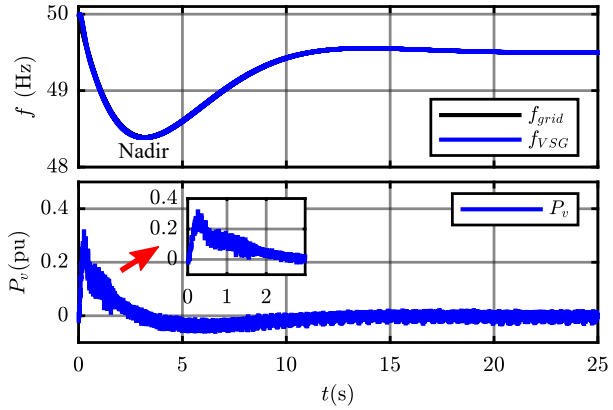

Fig. 14. Test 2: Inertial contribution of S-VSC during realistic grid frequency drop.
Top: Grid and S-VSC frequency (Hz); Bottom: Active power reference from S-VSC (pu).

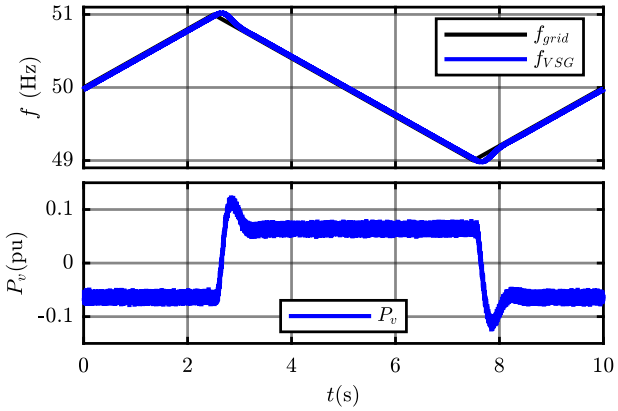

Fig. 15. Test 3: Inertial contribution of S-VSC. Grid frequency varies triangularly between 49 and 51 Hz with a period of 10 s.
Top: S-VSC frequency (Hz);Bottom: Active power reference from S-VSC (pu).

the S-VSC. As it can be seen in Fig. 14, the active power is injected transiently (first few seconds) to support the grid frequency. In the final stages of the fault, no power is injected, as the frequency derivative is null. An active droop controller can be added if the power plant where the VSG is implemented contributes to the primary regulation of the frequency. Thanks to the simplified damper implemented on the q-axis, the active droop and the damping feature are fully decoupled [15]. This aspect gives full freedom to chose the most appropriate active droop coefficients (usually in the range 2-5% [18]) without affecting the damping performance. In the second inertial test (Fig. 15) a triangular wave profile of the frequency has been imposed (± 1 Hz deviation from the rated 50 Hz with a period of 10 s). This

test clearly shows the inverse dependence of the active power injection from the grid frequency derivative. In fact, when the frequency rises (decreases) linearly, the active power injection is at a negative (positive) constant value and depends on the inertia constant H of the virtual machine.

C. Operating modes

The three defined operating modes (VSC, VSCap and VSG) have been compared in Tests 4, 5 and 6. First, in Tests 4 and 5, the identical step in the power references (from 0.1 pu to 0.2 pu) has been applied for each of the three operating modes and the results are compared in Fig. 16 and Fig. 17. Then, in Test 6 (Fig. 18), a simultaneous active and reactive power reference step (0.1 to 0.2 pu) has been applied. In these tests, no smoothing filter was applied to the calculated powers, therefore a substantial power ripple is visible. This power ripple is due to the measurement of the current i_{abc} and the grid voltage v_{pcc}. In fact, being the power the product of current and voltage, the measurement noise is amplified. Moreover, the measurement circuit was used far from its full range, being the power steps at few tens percent of the nominal power rating.

Test 4 (Fig. 16) compares both the VSM speed variation and the dynamic behavior of the active power injection, when a step in the active power reference is given (0.1 to 0.2 pu). The three operating modes are considered: VSC, VSCap and VSG. The VSC and VSCap show similar results, being the active power reference P^* directly fed to the inverter in both cases. In the last mode (VSG) the active power reference P^* is given to the VSM. The VSM has therefore to accelerate more to change its load angle δ, in order to transfer the required active power to the grid. A larger speed deviation Δf can be noted in Fig. 16. This has two detrimental effects. First, it slows down the dynamic power response of the inverter, as can be seen in Fig. 16, since the virtual rotor must modify its relative position to the grid angle. This is also beneficial when the virtual speed ω_r is used for grid frequency estimation, monitoring and as feedback for a basic proportional frequency regulation. Second, the machine stability is lowered, since the working point must move to a less stable position (see Fig. 6). Therefore, the VSC mode is the superior one, guaranteeing the desired active power flow with the fastest dynamics, higher damping ratio and the smallest speed variation. In summary, the proposed VSC operating mode is superior to the existing VSG/VSCap modes since it decouples the dynamic behavior of the inverter from the one of the VSM.

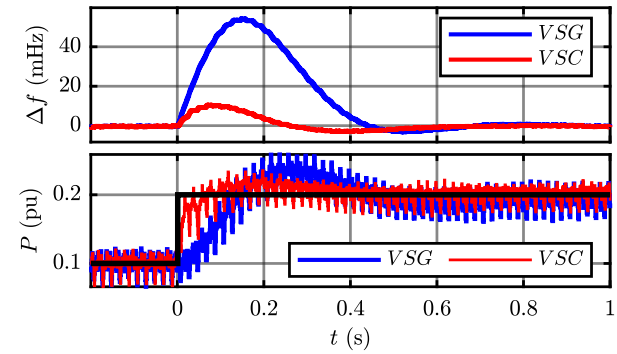

(a)

(b)

(c)

Fig. 16. Test 4: Active power reference P^* step (from 0.1 pu to 0.2 pu). Comparison of VSC/VSCap operating mode versus VSG mode. From top to bottom:
a) Frequency variation of the VSM (mHz) and active power injected by the inverter (pu);
b) Current waveforms for VSG mode. Ch2, phase voltage at the PCC (50 V / div). Ch5, phase current i_a (10 A / div);
c) Current waveforms for VSC/VSCap mode. Ch2, phase voltage at the PCC (50 V / div). Ch5, phase current i_a (10 A / div).

A similar test (Test 5) has been performed regarding the reactive power reference Q^*. The results are depicted in Fig. 17. In this case, the VSCap and VSG operating modes are equivalent, being the reactive power managed by the VSM in both cases. As in Test 3, also in this case the VSC mode is superior, guaranteeing a faster dynamic behavior, since the dynamic response does not depend on the machine parameters, but only on the design of the current control loop.

Finally, Test 5, where both the active and reactive power references are modified in VSC mode, has been performed. As per Fig. 18, little difference can be seen

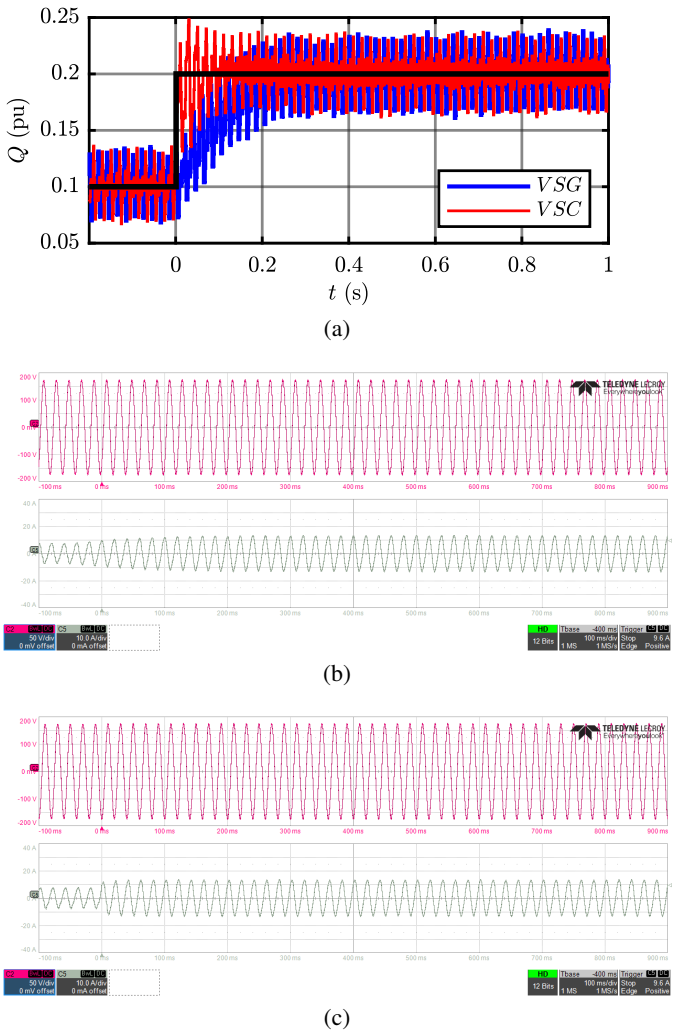

Fig. 17. Test 5: Reactive power reference Q^* step (from 0.1 pu to 0.2 pu). Comparison of VSC operating mode versus VSG/VSCap mode. From top to bottom:
a) Reactive power transient;
b) Current waveforms for VSG/VSCap mode. Ch2, phase voltage at the PCC (50 V / div). Ch5, phase current i_a (10 A / div);
c) Current waveforms for VSC mode. Ch2, phase voltage at the PCC (50 V / div). Ch5, phase current i_a (10 A / div).

from the previous tests 3 and 4, proving therefore that the two active and reactive power channels are well decoupled.

D. Grid Fault Tests

The S-VSC behavior in VSC mode in case of short circuits in the grid has been tested in tests 7, 8, 9 and 10 (shown in Figs. 19 to 22). Short circuits in the power system lead to voltage dips of various depth (depending on the grid reactance) seen by the generating unit. Therefore, voltage dip values suggested by the international grid standards were used first in Test 7. In particular, a 10 % voltage dip was applied by the grid emulator, emulating a CELL A5 dip according to EN50160. The results are available in Fig. 19. Two aspects must be

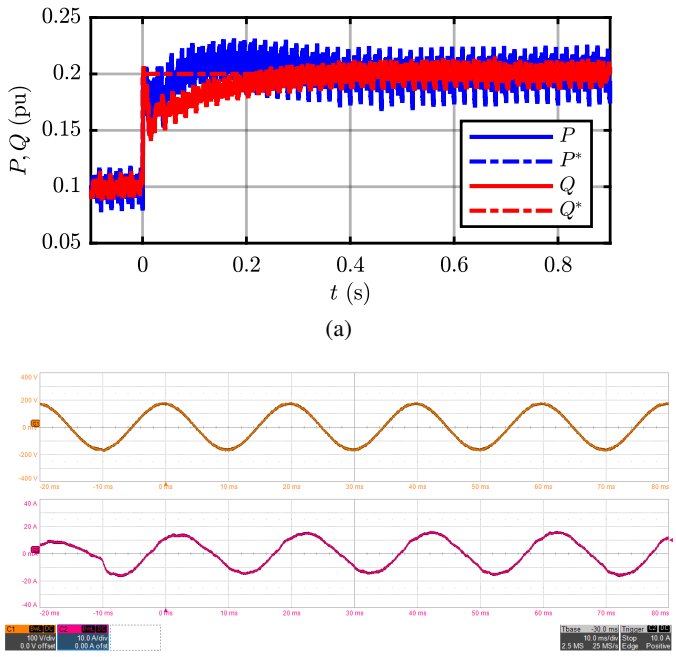

Fig. 18. Test 6: Active P^* and reactive Q^* power reference step (from 0.1 pu to 0.2 pu). From top to bottom:
a) Active and reactive power transient;
b) Ch1, phase voltage a at the PCC (100 V / div).
Ch2, phase current i_a (10 A / div).

noticed. First, the current limitation strategy described in Section III (Fig. 10), is effective. The current reference amplitude is saturated to the maximum set value (36 A in this test). The limitation is also proved by the current waveforms in Fig. 10b. Second, the inverter injects reactive current during the fault for grid support and protections triggering.

Tests 8, 9 and 10 deal with the excitation control and virtual parameters tuning. In these tests, the same perturbation has been applied from the grid emulator, i.e. a permanent voltage dip of 10 % with a phase jump of $-5°$. Three different sets of parameters have been tested.

In Test 8 (Fig. 20), the excitation control of the machine is enabled and therefore the machine provides full transient reactive support to the grid (i_q) with the set time constant $\tau_e = 0.1$ s. Moreover, the reference current is clamped to the limit value I_{max} (set to 36 A in such tests).

Test 9 (Fig. 21) demonstrates that permanent grid support can be provided if the excitation control is disabled (i.e. $k_e = 0$). In this case, the excitation flux linkage λ_e of the virtual machine is constant and equal to its value before the fault.

Test 10 (Fig. 22) shows the different behavior when changing the virtual stator resistance R_s. In this case, a much larger value has been selected ($R_s = 0.2$ pu). The virtual machine stator parameters R_s and L_s can

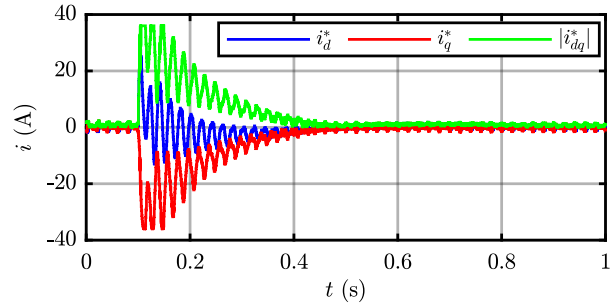

(a)

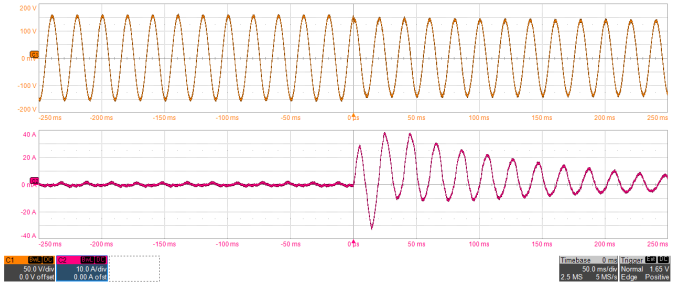

(b)

Fig. 19. Test 7: Voltage dip fault according to EN50160 (CELL A5 fault). Voltage dip from 92 % to 82 % of the nominal voltage. From top to bottom:
a) Inverter reference currents (A) in the (d,q) frame;
b) Ch1, voltage at PCC (50 V / div). Ch2, grid side phase current (10 A / div).

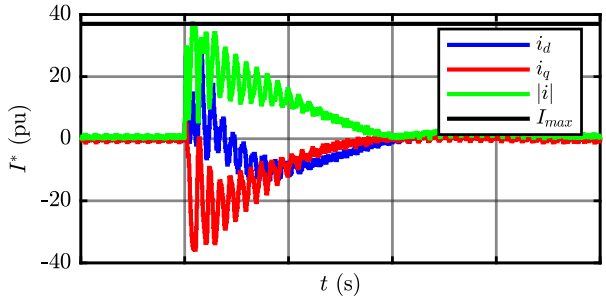

(a)

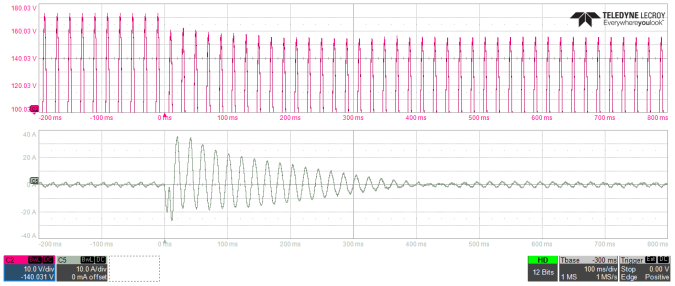

(b)

Fig. 20. Test 8: Voltage Dip Fault (-0.1 pu and −5°). S-VSC with excitation control enabled: τ_e = 0.1 s, R_s = 0.02 pu. Top to bottom:
a) Inverter currents (A) in the (d,q) frame;
b) Ch2, Positive envelope of the voltage at PCC (10 V / div). Ch5, phase current i_a (10 A / div).

be tuned to satisfy the needed support requirements in case of faults. While L_s regulates the magnitude of the transient support, R_s sets the damping of its response. As it can be seen in (Fig. 22), a higher resistance leads to a more damped transient after the fault occurred. This does not effect though the steady state operation, which is determined only by L_s and λ_e.

E. Tunable Harmonic Compensation

To prove the harmonic compensation capabilities, a distorted grid has been generated by means of the grid emulator. In particular, 5% 5th harmonic voltage distortion has been introduced. The system is operating at no load, so that the effect of the harmonic compensation can be highlighted.

The effect of the S-VSC is beneficial as results from the FFT analysis presented in Fig. 23. The 5th harmonic in the voltage has been attenuated from 6 V to 4 V, proving the effectiveness of the harmonic compensation feature. For better clarity, the current and voltage waveforms at the PCC are displayed in Fig. 24. The line-line voltage (yellow) shows the typical 5th harmonic distortion, which shaves the peaks of the voltage. When the S-VSC is off, the converter has no harmonic compensation

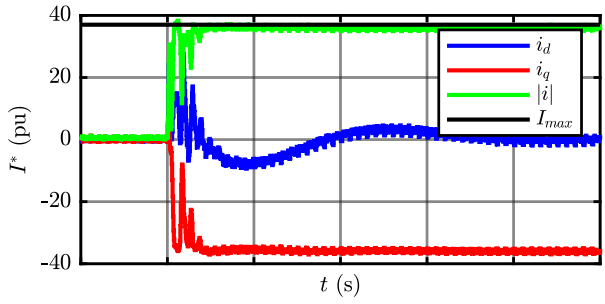

(a)

(b)

Fig. 21. Test 9: Voltage Dip Fault (-0.1 pu and −5°). R_s = 0.02 pu and excitation control disabled: k_e = 0. From top to bottom:
a) Inverter currents (A) in the (d,q) frame;
b) Ch2, Positive envelope of the voltage at PCC (10 V / div). Ch5, phase current i_a (10 A / div).

capability, therefore the injected current is near zero (Fig. 24a).

As soon as the S-VSC is switched on (Fig. 24b),

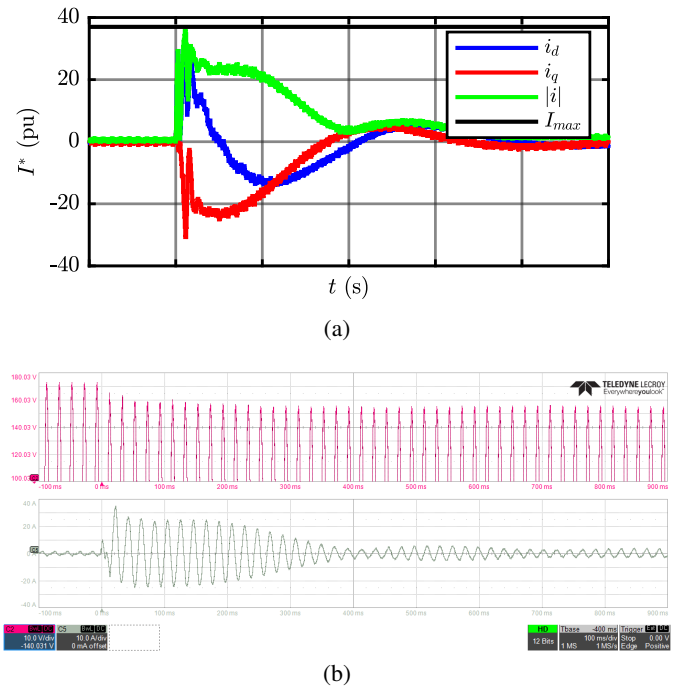

Fig. 22. Test 10: Voltage Dip Fault (-0.1 pu and $-5°$). VSG with large resistance R_s = 0.2 pu and excitation control enabled. From top to bottom:
a) Inverter currents (A) in the (d,q) frame;
b) Ch2, Positive envelope of the voltage at PCC (10 V / div). Ch5, phase current i_a (10 A / div).

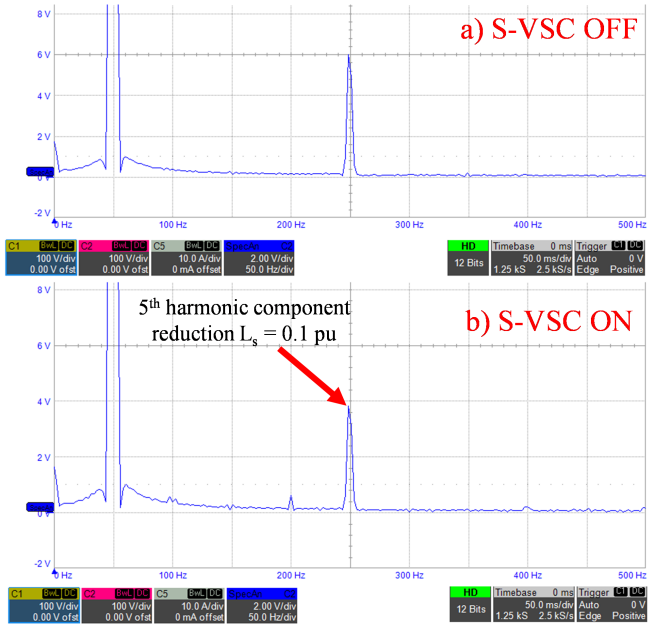

Fig. 23. Test 11: Harmonic compensation test. A 5% 5th harmonic component has been introduced into the emulated grid. A comparison with the S-VSC enabled and disabled is carried out. L_s = 0.1 pu. From top to bottom:
a) FFT of the voltage at the PCC when the S-VSC is off;
b) FFT of the voltage at the PCC when the S-VSC is on.

compensating current references are generated according to (7). The current contains a 5th harmonic component that contributes in reducing the magnitude of the voltage distortion. In this paper, the current control has been implemented in the (d,q) S-VSC frame using PI and resonant controllers on the 6th harmonic. Without such resonant controllers, the quality of the current reference tracking would have been much lower, thus decreasing the effectiveness of the harmonic compensation. It is therefore crucial to employ suitable current controller (e.g. resonant, MPC...) to ensure the correct tracking of the compensation current references.

As mentioned in Section II, the harmonic compensation is tunable and depends on the virtual inductance L_s of the stator. Therefore, a further test, has been performed using L_s = 0.05 pu. The FFT of the voltage at the PCC is shown in Fig. 25. The residual component of the 5th harmonic is 2.8 V. Comparing this result with the previous test (Fig. 23) it can be noted that the 5th harmonic is further reduced of 50%. This effect is proportional to the virtual stator inductance L_s. A smaller virtual stator inductance L_s will generate a larger compensation current and therefore a higher compensation effect according to (7).

V. Conclusions

In this paper an alternative approach to the integration of the virtual synchronous machine concept into the control of an inverter has been proposed and analyzed. The proposed approach, called S-VSC, only acts as a parallel compensator add-on and it is in charge of generating active and reactive power references for the inverter to provide ancillary services. These services include virtual inertia, reactive power support and current harmonic compensation, while a traditional current controlled inverter is in charge of injecting the desired active and reactive power into the grid. This way, the S-VSC is always operating at a very small load angle. Therefore, it presents very good performance in terms of transient stability and damping. Thanks to the virtual stator model, also voltage harmonics compensation is achieved.

The S-VSC model and integration has been presented and experimentally validated. The experimental results prove that a faster and more damped behavior in tracking the active power reference is obtained when the proposed approach is adopted. The grid ancillary services, such as virtual inertia, tunable reactive support to the grid and the tunable harmonic compensation, have also been demonstrated.

References

[1] IEA, “International Energy Agency (IEA) Energy Outlook 2019,” 2019.

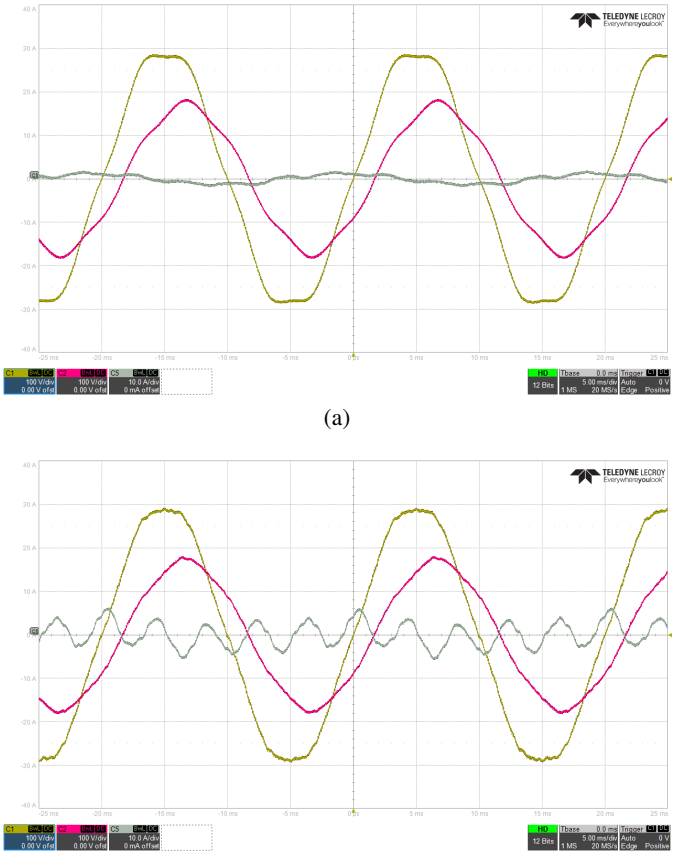

(a)

(b)

Fig. 24. Test 11: Harmonic compensation test. Current and voltage waveforms at PCC. C5 phase current (A), C2 phase voltage (V) and C1 line-line voltage (V). From top to bottom:
a) S-VSC is off;
b) S-VSC is on.

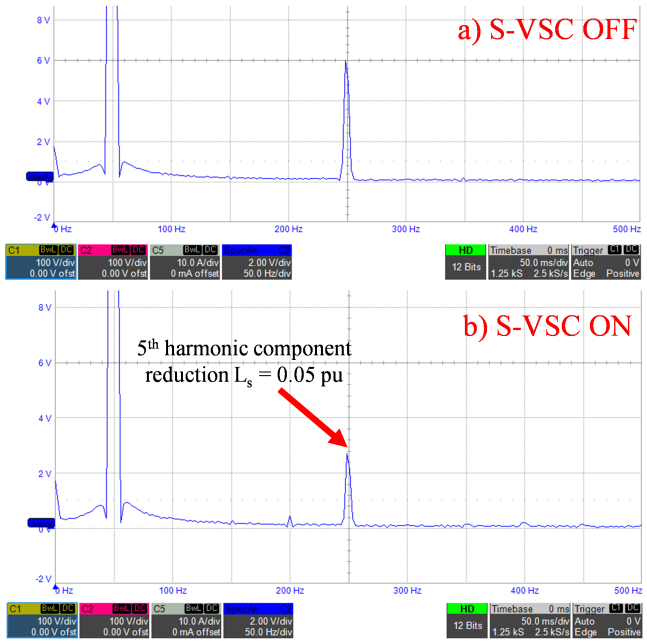

Fig. 25. Test 12: Harmonic compensation test. A 5% 5th harmonic component has been introduced into the emulated grid. A comparison with the S-VSC enabled and disabled is carried out. L_s = 0.05 pu. From top to bottom:
a) FFT of the voltage at the PCC when the S-VSC is off;
b) FFT of the voltage at the PCC when the S-VSC is on.

[2] J. Fang, H. Li, Y. Tang, and F. Blaabjerg, "On the Inertia of Future More-Electronics Power Systems," *IEEE Journal of Emerging and Selected Topics in Power Electronics*, vol. 7, pp. 2130–2146, Dec. 2019. Conference Name: IEEE Journal of Emerging and Selected Topics in Power Electronics.

[3] J. Rocabert, A. Luna, F. Blaabjerg, and P. Rodríguez, "Control of Power Converters in AC Microgrids," *IEEE Transactions on Power Electronics*, vol. 27, pp. 4734–4749, Nov. 2012.

[4] H.-P. Beck and R. Hesse, "Virtual synchronous machine," in *2007 9th International Conference on Electrical Power Quality and Utilisation*, pp. 1–6, Oct. 2007.

[5] R. Hesse, D. Turschner, and H.-P. Beck, "Micro grid stabilization using the virtual synchronous machine (VISMA)," *Renewable Energy and Power Quality Journal*, vol. 1, pp. 676–681, Apr. 2009.

[6] Y. Chen, R. Hesse, D. Turschner, and H.-P. Beck, "Dynamic Properties of the Virtual Synchronous Machine (VISMA)," *Renewable Energy and Power Quality Journal*, May 2011.

[7] Q.-C. Zhong and G. Weiss, "Synchronverters: Inverters That Mimic Synchronous Generators," *IEEE Transactions on Industrial Electronics*, vol. 58, pp. 1259–1267, Apr. 2011.

[8] Q. Zhong, P. Nguyen, Z. Ma, and W. Sheng, "Self-Synchronized Synchronverters: Inverters Without a Dedicated Synchronization Unit," *IEEE Transactions on Power Electronics*, vol. 29, pp. 617–630, Feb. 2014.

[9] S. D'Arco, J. A. Suul, and O. B. Fosso, "A Virtual Synchronous Machine implementation for distributed control of power converters in SmartGrids," *Electric Power Systems Research*, vol. 122, pp. 180–197, May 2015.

[10] J. Driesen and K. Visscher, "Virtual synchronous generators," in *2008 IEEE Power and Energy Society General Meeting - Conversion and Delivery of Electrical Energy in the 21st Century*, pp. 1–3, July 2008.

[11] H. Bevrani, T. Ise, and Y. Miura, "Virtual synchronous generators: A survey and new perspectives," *International Journal of Electrical Power & Energy Systems*, vol. 54, pp. 244–254, Jan. 2014.

[12] P. Rodríguez, C. Citro, J. I. Candela, J. Rocabert, and A. Luna, "Flexible Grid Connection and Islanding of SPC-Based PV Power Converters," *IEEE Transactions on Industry Applications*, vol. 54, pp. 2690–2702, May 2018.

[13] W. Zhang, A. M. Cantarellas, J. Rocabert, A. Luna, and P. Rodriguez, "Synchronous Power Controller With Flexible Droop Characteristics for Renewable Power Generation Systems," *IEEE Transactions on Sustainable Energy*, vol. 7, pp. 1572–1582, Oct. 2016.

[14] W. Zhang, A. Tarraso, J. Rocabert, A. Luna, J. I. Candela, and P. Rodriguez, "Frequency Support Properties of the Synchronous Power Control for Grid-Connected Converters," *IEEE Transactions on Industry Applications*, vol. 55, pp. 5178–5189, Sept. 2019.

[15] F. Mandrile, E. Carpaneto, and R. Bojoi, "Virtual Synchronous Generator with Simplified Single-Axis Damper Winding," in *2019 IEEE 28th International Symposium on Industrial Electronics (ISIE)*, pp. 2123–2128, June 2019.

[16] F. Mandrile, E. Carpaneto, and R. Bojoi, "Grid-Tied Inverter with Simplified Virtual Synchronous Compensator for Grid Services and Grid Support," in *2019 IEEE Energy Conversion Congress and Exposition (ECCE)*, pp. 4317–4323, Sept. 2019.

[17] Y. Hirase, K. Abe, K. Sugimoto, and Y. Shindo, "A grid-connected inverter with virtual synchronous generator model

of algebraic type," *Electrical Engineering in Japan*, vol. 184, no. 4, pp. 10–21, 2013.
[18] P. Kundur, *Power System Stability and Control*. McGraw-Hill Education, Jan. 1994.
[19] R. Teodorescu, M. Liserre, and P. Rodriguez, *Grid Converters for Photovoltaic and Wind Power Systems*. John Wiley & Sons, July 2011.
[20] F. Blaabjerg, R. Teodorescu, M. Liserre, and A. V. Timbus, "Overview of Control and Grid Synchronization for Distributed Power Generation Systems," *IEEE Transactions on Industrial Electronics*, vol. 53, pp. 1398–1409, Oct. 2006.
[21] R. I. Bojoi, G. Griva, V. Bostan, M. Guerriero, F. Farina, and F. Profumo, "Current control strategy for power conditioners using sinusoidal signal integrators in synchronous reference frame," *IEEE Transactions on Power Electronics*, vol. 20, pp. 1402–1412, Nov. 2005.

Fabio Mandrile (S'18) received the B.Sc. and M.Sc. degrees in electrical engineering in 2015 and 2017, respectively, from Politecnico di Torino, Torino, Italy, where he is currently working toward the Ph.D. degree in Electrical Engineering. His main research interests include Virtual Synchronous Generators and power electronics for grid-connected applications.

Enrico Carpaneto (M'86) was born in Torino, Italy, in 1959. He received the M.Sc. and Ph.D. degrees in electrical engineering from Politecnico di Torino, Torino, Italy, in 1984 and 1989, respectively. He is currently an Associate with the Energy Department, Politecnico di Torino. His research activities cover many different aspects of modeling, simulation and optimization of generation, transmission and distribution systems. He has published more than 100 scientific papers. He has been responsible for several research contracts concerning analysis, operation and planning of distribution networks, power quality, and generation optimization. His current research interests include distribution systems, dispersed generation, virtual synchronous generators, and thermal models. Dr. Carpaneto is a member of the IEEE Power Engineering Society and Associazione Italiana di Elettrotecnica, Elettronica, Automazione, Informatica e Telecomunicazioni (AEIT)

Radu Bojoi (SM'10, F'19) received the MSc degree in Electrical Engineering from Technical University of Iasi, Romania, in 1993, and the Ph.D. in Electrical Engineering from Politecnico di Torino, Italy, in 2002. He is a Full Professor of Power Electronics and Electrical Drives in the Energy Department "G. Ferraris" and Chairman of the Power Electronics Innovation Center at Politecnico di Torino, Italy. Dr. Bojoi published more than 150 papers covering electrical drives and power electronics for industrial applications, transportation electrification, power quality, and home appliances. He was involved in many research projects with industry for direct technology transfer aiming at obtaining new products. Dr. Bojoi is the co-recipient of 5 prize paper awards, the last one in 2015 as IEEE-IAS Prize Paper Award. Dr. Bojoi is a Co-Editor-In-Chief of the IEEE Transactions on Industrial Electronics and Chair of the Electrical Machines Technical Committee of the Industrial Electronics Society.